

RESEARCH ARTICLE | AUGUST 07 2024


Toward large eddy simulation of shear-thinning liquid jets: A *priori* analysis of subgrid scale closures for multiphase flows

M. Abdelsayed   ; J. Hasslberger  ; M. Ertl  ; B. Weigand  ; M. Klein 



Physics of Fluids 36, 085130 (2024)

<https://doi.org/10.1063/5.0219269>





Physics of Fluids

Special Topic:
Flow and Climate

Guest Editors: Khaled Ghannam and Mostafa Momen

[Submit Today!](#)



Toward large eddy simulation of shear-thinning liquid jets: *A priori* analysis of subgrid scale closures for multiphase flows

Cite as: Phys. Fluids **36**, 085130 (2024); doi: 10.1063/5.0219269

Submitted: 16 May 2024 · Accepted: 22 July 2024 ·

Published Online: 7 August 2024



View Online



Export Citation



CrossMark

M. Abdelsayed,^{1,a)} J. Hasslberger,¹ M. Ertl,² B. Weigand,² and M. Klein¹

AFFILIATIONS

¹Department of Aerospace Engineering, Institute of Applied Mathematics and Scientific Computing, University of the Bundeswehr Munich, Werner-Heisenberg-Weg 39, 85577 Neubiberg, Germany

²Institute of Aerospace Thermodynamics, University of Stuttgart, Pfaffenwaldring 31, 70569 Stuttgart, Germany

^{a)}Author to whom correspondence should be addressed: marianne.abdelsayed@unibw.de

ABSTRACT

While direct numerical simulation (DNS) of multiphase flows has been the focus of many research investigations in recent years, large eddy simulation (LES) of multiphase flows remains a challenge. There is no standardized set of governing equations for multiphase LES. Different approaches and formulations have been discussed in the literature, each with its own advantages and disadvantages. In this paper, the conventional (non-weighted) filtering approach is compared with the density-weighted Favre filtering method by evaluating the subgrid scale (SGS) energy transfer for a simple test case of a shear-thinning droplet in air. The findings reveal that, unlike the Favre filtering approach, the conventional filtering method results in a notable amount of nonphysical backward scatter in the flow. Based on these results, the Favre filtering method appears preferable and is applied to the *a priori* analysis of shear-thinning liquid jets, where the viscosity has been modeled using the Carreau–Yasuda model. First, by explicitly filtering existing DNS data of shear-thinning jet breakup into stagnant air, the order of magnitude of different SGS terms is evaluated using the Favre filtering method. Consistent with earlier studies on Newtonian jets, the present study indicates that the diffusive term remains negligible, while the convective term plays a dominant role. Functional and structural models for the closure of the convective SGS term are assessed by means of a correlation analysis and an order of magnitude study. Existing structural models provide good results for both Newtonian and shear-thinning cases. Promising *a posteriori* model candidates are discussed.

© 2024 Author(s). All article content, except where otherwise noted, is licensed under a Creative Commons Attribution (CC BY) license (<https://creativecommons.org/licenses/by/4.0/>). <https://doi.org/10.1063/5.0219269>

I. INTRODUCTION

Atomization is ubiquitous in various technical applications, such as fuel injection, spray painting, and spray drying, as well as in natural processes, such as waterfalls and breaking ocean waves.¹ In many technical processes, particularly in spray painting and agricultural processes, non-Newtonian fluids are involved. However, compared to Newtonian jets, the dynamics of non-Newtonian jets remain incompletely understood, particularly regarding their modeling in the presence of turbulence.

Due to significant improvements in computing power in recent years, DNS of complex multiphase flows at moderate Reynolds and Weber numbers has become feasible. Extensive research has been devoted to the atomization process of Newtonian jets, with significant focus on the primary atomization process of diesel-like sprays.^{2–7} A few studies focused on non-Newtonian sprays. Ertl and Weigand⁸

investigated several shear-thinning jets, analyzing the effect of different inlet velocity profiles on the primary breakup. A novel breakup mechanism for shear-thinning jets, termed cavity breakup, is identified by Zhu *et al.*⁹ This mechanism originates from the roll-up of interfacial waves, forming a cavity structure on the interface that further disintegrates into droplets and ligaments. A turbulent transition due to elastic instability in planar jets at low Reynolds numbers is observed by Soligo and Rosti.¹⁰ Guimarães *et al.*¹¹ compared several turbulent viscoelastic jets with a reference Newtonian jet, demonstrating that viscoelastic jets exhibit slower spreading and decay rates.

In many industrial applications, where atomization is characterized by high Reynolds and Weber numbers, DNS is not feasible anymore. LES is a good compromise between DNS and Reynolds-averaged Navier–Stokes (RANS) based approaches regarding computational cost and accuracy. While LES of Newtonian single-phase flows

is well established, LES of multiphase flows is still in an early development phase as it involves additional unclosed terms. Fundamental work on governing equations for LES of multiphase flows was carried out by Labourasse *et al.*,¹² Liovic and Lakehal,¹³ and Toutant *et al.*¹⁴ Various formulations of the LES governing equations exist in the literature, based on the conventional (non-weighted) filtering and Favre averaging using the one-fluid approach, as well as the multi-fluid formulation. Several *a priori* studies have estimated the order of magnitude of the SGS terms in academic test cases,^{14,15} as well as jet atomization,^{5,16} emphasizing their importance for accurate multiphase LES.

A few models have been proposed for SGS terms arising solely for multiphase flows, particularly the surface tension SGS term. Aniszewski *et al.*¹⁷ applied the approximate deconvolution approach of Stolz and Adams¹⁸ to close the surface tension SGS term. This approach has been applied later by Saeedipour *et al.*¹⁹ to all unclosed terms in an *a posteriori* study. Saeedipour and Schneiderbauer²⁰ included surface tension in the subgrid eddy viscosity by a correction term. A variety of models for the various SGS terms were tested by Ketterl and Klein³ and Klein *et al.*⁵ *A priori* assessment of surface tension and interfacial SGS terms was conducted by Hasslberger *et al.*²¹ Ketterl *et al.*²² demonstrated the influence of SGS surface tension on the interface dynamics in *a posteriori* studies.

Overall, progress in non-Newtonian LES remains limited. A few studies focused on either deriving or adapting existing SGS closure models for non-Newtonian single-phase flows. One of the pioneering studies to explore additional non-Newtonian SGS terms was conducted by Ohta and Miyashita,²³ focusing on viscous, inelastic non-Newtonian fluids. Their findings suggest that the non-Newtonian SGS (NNSGS) term might be negligible. Moreover, they proposed an extended Smagorinsky model for the closure of the convective SGS term in wall-bounded flows, accounting for viscosity changes using a damping function. Following the findings of Ohta and Miyashita,²³ Gnambode *et al.*²⁴ neglected the additional NNSGS term for LES of turbulent pipe flow using various shear-thinning and shear-thickening fluids. Amani *et al.*²⁵ proposed dynamic models for the closure of the NNSGS term for viscous, inelastic non-Newtonian fluids. In the case of viscoelastic fluids, several studies have explored and evaluated additional terms resulting from the presence of polymers in the fluid.^{26–28}

Given the important role non-Newtonian sprays play in technical processes and the relatively sparse research in this regard, it is evident, that there exists a pressing need to investigate SGS terms for non-Newtonian LES of multiphase flows. Understanding the interaction between turbulent structures and rheological properties is essential for accurately predicting non-Newtonian multiphase flow behavior. Thus, the aim of this paper is threefold:

1. Analyze the SGS energy transfer using conventional and Favre filtering in order to identify which approach is better aligned with common LES modeling assumptions;
2. Investigate the order of magnitude of the diffusive and convective SGS terms and identify differences and commonalities between non-Newtonian and Newtonian jets, particularly highlighting the physics of the unclosed terms at the interface;
3. Assess a variety of functional and structural closure models for the convective SGS term.

The remainder of the paper is organized as follows. The LES governing equations for multiphase flows using the one-fluid formulation

are introduced in Sec. II. In Sec. III, the SGS energy transfer is analyzed using different filtering approaches. Further, SGS closure models are presented in Sec. IV, followed by an *a priori* analysis of shear-thinning jets in Sec. V. Finally, Sec. VI provides a summary of the findings. A table of the nomenclature is included at the end of the paper.

II. LES GOVERNING EQUATIONS

A two-phase flow system of two immiscible, incompressible fluids can be described using the one-fluid formulation of the Navier–Stokes equations consisting of the continuity equation and the momentum equation²⁹

$$\frac{\partial u_i}{\partial x_i} = 0, \tag{1}$$

$$\frac{\partial \rho u_i}{\partial t} + \frac{\partial \rho u_i u_j}{\partial x_j} = -\frac{\partial p}{\partial x_i} + \frac{\partial}{\partial x_j} \left[\mu \left(\frac{\partial u_i}{\partial x_j} + \frac{\partial u_j}{\partial x_i} \right) \right] + \Gamma n_i \kappa \delta_S. \tag{2}$$

Here, u_i are the velocity components, ρ is the density, p is the pressure, μ is the dynamic viscosity, Γ is the surface tension coefficient, n_i is the unit vector normal to the interface, κ is the local interface curvature, δ_S is the interface indicator function, and the subscripts $i, j = 1, 2, 3$ represent the Cartesian indices. In the volume of fluid (VOF)³⁰ context, the local volume fraction α

$$\alpha = \begin{cases} 0 & \text{in gaseous phase,} \\]0, 1[& \text{in interface cells,} \\ 1 & \text{in liquid phase,} \end{cases} \tag{3}$$

is used for the calculation of local material properties, such as density and dynamic viscosity by linear interpolation, resulting in

$$\rho = \alpha \rho_l + (1 - \alpha) \rho_g, \quad \mu = \alpha \mu_l + (1 - \alpha) \mu_g. \tag{4}$$

Here, the indices g and l correspond to the gas and liquid phase, respectively. The volume fraction α is advected using the following equation:

$$\frac{\partial \alpha}{\partial t} + \frac{\partial \alpha u_i}{\partial x_i} = 0. \tag{5}$$

To derive the LES governing equations, a spatial low-pass filter is applied to any field variable ϕ as defined by Sagaut³¹

$$\bar{\phi}(\mathbf{x}) = G * \phi = \int \phi(\mathbf{y}) G(\mathbf{x} - \mathbf{y}) d\mathbf{y}. \tag{6}$$

Here, G is the Gaussian filter kernel

$$G(x_i) = \left(\frac{6}{\pi \Delta^2} \right)^{1/2} \exp\left(-\frac{6x_i^2}{\Delta^2}\right), \tag{7}$$

$$G(x, y, z) = G(x)G(y)G(z).$$

For variable density flows, such as compressible flows or reacting flows, the density-weighted filtering, i.e., Favre filtering, is defined as³²

$$\tilde{\phi} = \frac{\overline{\rho \phi}}{\bar{\rho}}. \tag{8}$$

In the context of multiphase flows, the Favre filtering method was introduced by Labourasse *et al.*,¹² Liovic and Lakehal,^{13,33} and Toutant

*et al.*¹⁴ The Favre filtering approach has the advantage, that additional unclosed correlations between density and any arbitrary additional variable ϕ can be avoided. However, the Favre filtering does not commute with differentiation in time $\frac{\partial \tilde{\phi}}{\partial t} \neq \frac{\partial \phi}{\partial t}$ and in space $\frac{\partial \tilde{\phi}}{\partial x_i} \neq \frac{\partial \phi}{\partial x_i}$. Additionally, it does not commute with averaging $\langle \tilde{\phi} \rangle \neq \langle \phi \rangle$.³⁴ Moreover, there is no simple relation between $\tilde{\phi}$ and ϕ and comparison of numerical simulations and experimental data is not obvious, as numerical simulations give density-weighted filtered quantities.³⁵

By applying the filtering operation [Eq. (6)] to Eqs. (1), (2), and (5), the LES governing equations using the one-fluid formulation are given as

$$\frac{\partial \bar{u}_i}{\partial x_i} = 0, \quad (9)$$

$$\frac{\partial \bar{\rho} \bar{u}_i}{\partial t} + \frac{\partial \bar{\rho} \bar{u}_i \bar{u}_j}{\partial x_j} = -\frac{\partial \bar{p}}{\partial x_i} + \frac{\partial}{\partial x_j} \left[\bar{\mu} \left(\frac{\partial \bar{u}_i}{\partial x_j} + \frac{\partial \bar{u}_j}{\partial x_i} \right) \right] + \Gamma \bar{\kappa} \bar{n}_i \bar{\delta}_S + \tau_{nn,i} - \frac{\partial}{\partial t} \tau_{tt,i} - \frac{\partial}{\partial x_j} \tau_{\rho uu,ij} + \frac{\partial}{\partial x_j} \tau_{\mu S,ij}, \quad (10)$$

$$\frac{\partial \bar{\alpha}}{\partial t} + \frac{\partial \bar{\alpha} \bar{u}_i}{\partial x_i} = -\frac{\partial}{\partial x_i} \tau_{\alpha u,i}. \quad (11)$$

The filtering operation results in five unclosed subgrid terms, i.e., the convective SGS term

$$\tau_{\rho uu,ij} = \overline{\rho u_i u_j} - \bar{\rho} \bar{u}_i \bar{u}_j, \quad (12)$$

the diffusive SGS term

$$\tau_{\mu S,ij} = \mu \left(\frac{\partial u_i}{\partial x_j} + \frac{\partial u_j}{\partial x_i} \right) - \bar{\mu} \left(\frac{\partial \bar{u}_i}{\partial x_j} + \frac{\partial \bar{u}_j}{\partial x_i} \right), \quad (13)$$

the surface tension SGS term

$$\tau_{nn,i} = \Gamma \bar{\kappa} \bar{n}_i \bar{\delta}_S - \Gamma \bar{\kappa} \bar{n}_i \bar{\delta}_S, \quad (14)$$

the acceleration SGS term

$$\tau_{tt,i} = \overline{\rho u_i} - \bar{\rho} \bar{u}_i, \quad (15)$$

and the interfacial SGS term

$$\tau_{\alpha u,i} = \overline{\alpha u_i} - \bar{\alpha} \bar{u}_i. \quad (16)$$

Using the Favre filtering operation given in Eq. (8), the LES equations read^{12,14}

$$\frac{\partial \tilde{u}_i}{\partial x_i} = \tau_{div}, \quad (17)$$

$$\frac{\partial \bar{\rho} \tilde{u}_i}{\partial t} + \frac{\partial \bar{\rho} \tilde{u}_i \tilde{u}_j}{\partial x_j} = -\frac{\partial \bar{p}}{\partial x_i} + \frac{\partial}{\partial x_j} \left[\bar{\mu} \left(\frac{\partial \tilde{u}_i}{\partial x_j} + \frac{\partial \tilde{u}_j}{\partial x_i} \right) \right] + \Gamma \bar{n}_i \bar{\kappa} \bar{\delta}_S + \tau_{nn,i} - \frac{\partial}{\partial x_j} \tau_{\rho uu,ij} + \frac{\partial}{\partial x_j} \tau_{\mu S,ij}, \quad (18)$$

$$\frac{\partial \bar{\alpha}}{\partial t} + \frac{\partial \bar{\alpha} \tilde{u}_i}{\partial x_i} = 0. \quad (19)$$

In the context of Favre filtering, the SGS terms can be expressed as

$$\tau_{div} = \frac{\rho_l - \rho_g}{\bar{\rho}} \left(\frac{\partial \alpha}{\partial x_i} u_i - \frac{\partial \alpha}{\partial x_i} \tilde{u}_i \right), \quad (20)$$

$$\tau_{\rho uu,ij} = \bar{\rho} (\tilde{u}_i \tilde{u}_j - \tilde{u}_i \tilde{u}_j), \quad (21)$$

$$\tau_{\mu S,ij} = \mu \left(\frac{\partial u_i}{\partial x_j} + \frac{\partial u_j}{\partial x_i} \right) - \bar{\mu} \left(\frac{\partial \tilde{u}_i}{\partial x_j} + \frac{\partial \tilde{u}_j}{\partial x_i} \right), \quad (22)$$

$$\tau_{nn,i} = \Gamma \bar{n}_i \bar{\kappa} \bar{\delta}_S - \Gamma \bar{n}_i \bar{\kappa} \bar{\delta}_S. \quad (23)$$

In contrast to the conventional filtering method, there is no temporal SGS term in the Favre filtering approach. However, the divergence-free assumption of the filtered velocities does not hold true anymore.

III. COMPARISON OF DIFFERENT FILTERING APPROACHES

As the governing equations for multiphase LES are not fully established yet,⁵ we assess different filtering approaches, i.e., conventional filtering and Favre filtering by comparing the SGS energy transfer in both cases. The SGS energy transfer is a fundamental parameter in LES. Following the concept of an energy cascade as introduced by Richardson,³⁶ kinetic energy feeds the turbulent energy cascade through the largest scales of motion and is transferred to smaller scales. At the smallest scales, the energy is dissipated. Locally, energy can be transferred from smaller to larger scales, while the mean dissipation follows the energy cascade.

The SGS energy transfer is investigated using a configuration with reduced complexity in terms of interface topology and turbulence homogeneity. The analysis focuses on a shear-thinning droplet in air, which is characterized by a reasonable complexity of the interface and a sufficient dynamic range for filtering. The droplet represents a single, isolated, and very well-resolved droplet of the liquid spray.

A. Numerical method and setup

The analysis is performed using the state-of-the-art open-source multiphase code “PARALLEL ROBUST INTERFACE SIMULATOR” (PARIS).³⁷ The finite-volume based code solves the incompressible Navier–Stokes equations on a staggered grid based on the one-fluid formulation. The interface between the phases is captured using the VOF method, and the volume fraction function is advected using the calcul d’interface affine par morceaux (CIAM) scheme.³⁸ A second-order time discretization scheme is used, while the Quadratic Upstream Interpolation for Convective Kinematics (QUICK) scheme is employed for the convective term of the momentum equation. The diffusive term of the momentum equation is discretized using the central differencing scheme. The system of equations is solved in the framework of the projection method. A multigrid Poisson solver provided by the HYPRE library is used for the calculation of the pressure field.

The computational setup is a shear-thinning droplet (Praestol 2500 0.3%,⁸ denoted as P2500 0.3% later) in turbulent air flow ($D_{\text{drop}} = 5$ mm) in a triply periodic box with a domain length of $L = 10$ mm. The surface tension coefficient at the liquid–air interface is $\Gamma = 73.15$ mN/m. The drop Reynolds number is $Re = u_{x,\text{rel}} D_{\text{drop}} \rho_g / \mu_g \approx 2700$, where $u_{x,\text{rel}} = \langle u_x \rangle_l - \langle u_x \rangle_g \approx 8.3$ m/s is the relative velocity in axial direction, where the gravitational force ($g_x = 9.81$ m/s²) is acting. The mesh is cubic and equidistant with a grid resolution of $\Delta = D_{\text{drop}}/128$. Following the definition of Koebe *et al.*,³⁹ the Kolmogorov length scale $\eta_K = (\nu^3/\varepsilon)^{1/4}$ can be estimated using

TABLE I. Shear-thinning droplet: overviews of the material properties.

Fluid	ρ (kg/m ³)	μ_0 (Pa s)	μ_∞ (Pa s)	λ (s)	a (-)	n (-)
P2500 0.3%	999.4	0.046	0.004	0.157	1.036	0.576
Air	1.189	$1.82 \cdot 10^{-5}$	-	-	-	-

$\nu = \nu_g$ and $\varepsilon \approx u_{x,rel} g_x$, which yields $\eta_K = 2.08 \cdot \Delta$. The Carreau-Yasuda viscosity model, as given by Tanner,⁴⁰ was used to model the shear-thinning behavior of the liquid phase:

$$\mu_l(\dot{\gamma}) = \mu_\infty + (\mu_0 - \mu_\infty) [1 + (\lambda \dot{\gamma})^a]^{(n-1)/a}. \quad (24)$$

Here, μ_0 is the first Newtonian plateau, μ_∞ is the second Newtonian plateau, $\dot{\gamma} = \sqrt{2S_{ij}S_{ij}}$ is the shear rate, S_{ij} is the strain rate tensor, λ is the characteristic time, n is the power-law index, and a describes the transition between the Newtonian plateau and power-law region. The material properties⁸ are summarized in Table I. A visualization of the test case is given as an isocontour at $\alpha = 0.5$, see Fig. 1.

B. Results and discussion

The DNS data have been explicitly filtered using a Gaussian filter kernel in the case of conventional filtering. For the Favre filtering, the filtered data have been additionally phase-weighted. The filtered dataset has the same dimensions as the DNS field. Gradients of the filtered DNS data are evaluated based on the coarse LES grid size $\Delta = n\Delta_{DNS}$ using a second order finite difference formula. The field of view for the analysis corresponds to the snapshot provided in Fig. 1. For the analysis, a single time step was taken after a statistically steady-state has been achieved.

In the conventional (Favre) filtering approach, the SGS energy transfer is defined as $\varepsilon_{SGS} = \tau_{ij}\tilde{S}_{ij}$ ($\varepsilon_{SGS} = \tau_{ij}\tilde{S}_{ij}$), where $\tau_{ij} = \overline{\rho u_i u_j} - \rho \tilde{u}_i \tilde{u}_j$ ($\tau_{ij} = \overline{\rho(u_i \tilde{u}_j - \tilde{u}_i \tilde{u}_j)}$) is the SGS term obtained from the

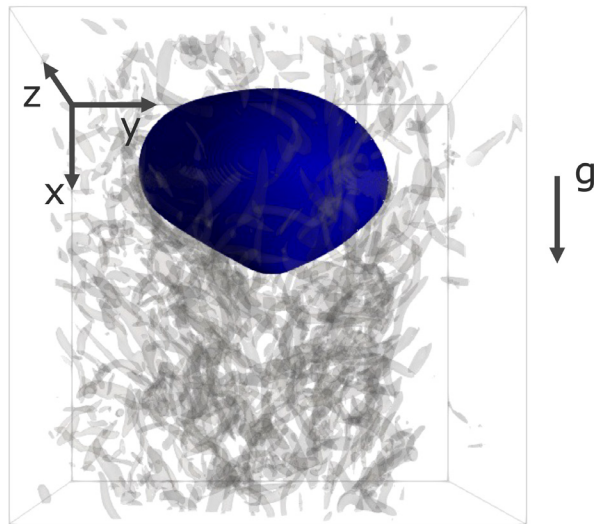


FIG. 1. Isocontour of shear-thinning droplet in air at $\alpha = 0.5$ (blue) in turbulent flow. Flow structures are visualized using the isosurfaces from Q-criterion at $Q = 3 \times 10^8 \text{ s}^{-2}$ (gray).

filtered DNS and $\tilde{S}_{ij} = 1/2(\partial \tilde{u}_i / \partial x_j + \partial \tilde{u}_j / \partial x_i)$ ($\tilde{S}_{ij} = 1/2(\partial \tilde{u}_i / \partial x_j + \partial \tilde{u}_j / \partial x_i)$) is the filtered strain rate tensor. The SGS energy transfer is assessed for a variety of filter widths $\Delta / \Delta_{DNS} = 2, 4,$ and 8 across different flow regions as indicated by the filtered volume fraction $\bar{\alpha}$. The flow domain $\bar{\alpha} = [0, 1]$ is subdivided in five equally spaced regions. Here, $\bar{\alpha} = 0$, $\bar{\alpha} = 0.5$, and $\bar{\alpha} = 1$ denote the gas bulk flow, the interface and liquid bulk flow, respectively. Figure 2 depicts the mean SGS energy transfer plotted against the filtered volume fraction $\bar{\alpha}$. Additionally, the contributions of mean positive energy transfer (backward scatter) and mean negative energy transfer (forward scatter) are plotted.

The conventional filtering method results in a dominating amount of backward scatter at all examined filter widths, leading to a positive mean energy transfer in the flow. In contrast, the amount of negative SGS energy transfer in the flow is low. Generally, the SGS energy transfer increases with increasing filter width. The conventional filtering method results in a significantly higher amount of both positive and negative SGS energy transfer compared to the Favre filtering approach.

The density-weighted filtering leads to a moderate amount of backward scatter in the flow compared to the mean forward scatter for all investigated filter widths. As a result, the mean SGS energy transfer in the flow is negative. Both the negative and positive SGS energy transfer increase at higher filter widths. Similar results have been obtained for a Newtonian case consisting of a falling water droplet in air, which is not shown here. The results are more physically plausible compared to the conventional filtering. Consequently, the Favre filtering approach will be used in the following analysis, as it appears to be better in line with conventional modeling assumptions, as well as physical expectations. It should be noted, that both filtering approaches lead to minimal backward scatter in the liquid and gas bulk phases, which is not shown in Fig. 2.

IV. SGS CLOSURE MODELS

In this section, SGS closure models are only presented in the context of Favre filtering, as it is more suitable for this specific case than the conventional filtering method, see Sec. III. The analysis in Sec. V B reveals, that the diffusive term remains relatively small compared to the convective term. Further, the interfacial term does not contain any features that would be specific to non-Newtonian flows. Therefore, only the modeling of the convective term will be addressed in detail. Two eddy viscosity (EV) and two structural models are presented for the closure of the convective SGS term.

EV models only model the deviatoric part of the SGS stress tensor and rely on the theory of Boussinesq, which states that momentum transfer in turbulent flows can be modeled using a turbulent viscosity ν_t , as defined by

$$\tau_{\rho uu,ij}^{EV} = \tau_{ij} - \frac{1}{3} \tau_{kk} \delta_{ij} = -2\bar{\rho} \nu_t \tilde{S}_{ij}. \quad (25)$$

Among the EV models, the standard Smagorinsky model⁴¹ (S) is often used for the closure of the convective SGS stress term. The underlying assumption of EV models is that the balance of the mean energy transfer alone between resolved and unresolved scales is sufficient to describe the action of the subgrid scales, together with the hypothesis that the transfer mechanism from the resolved to the

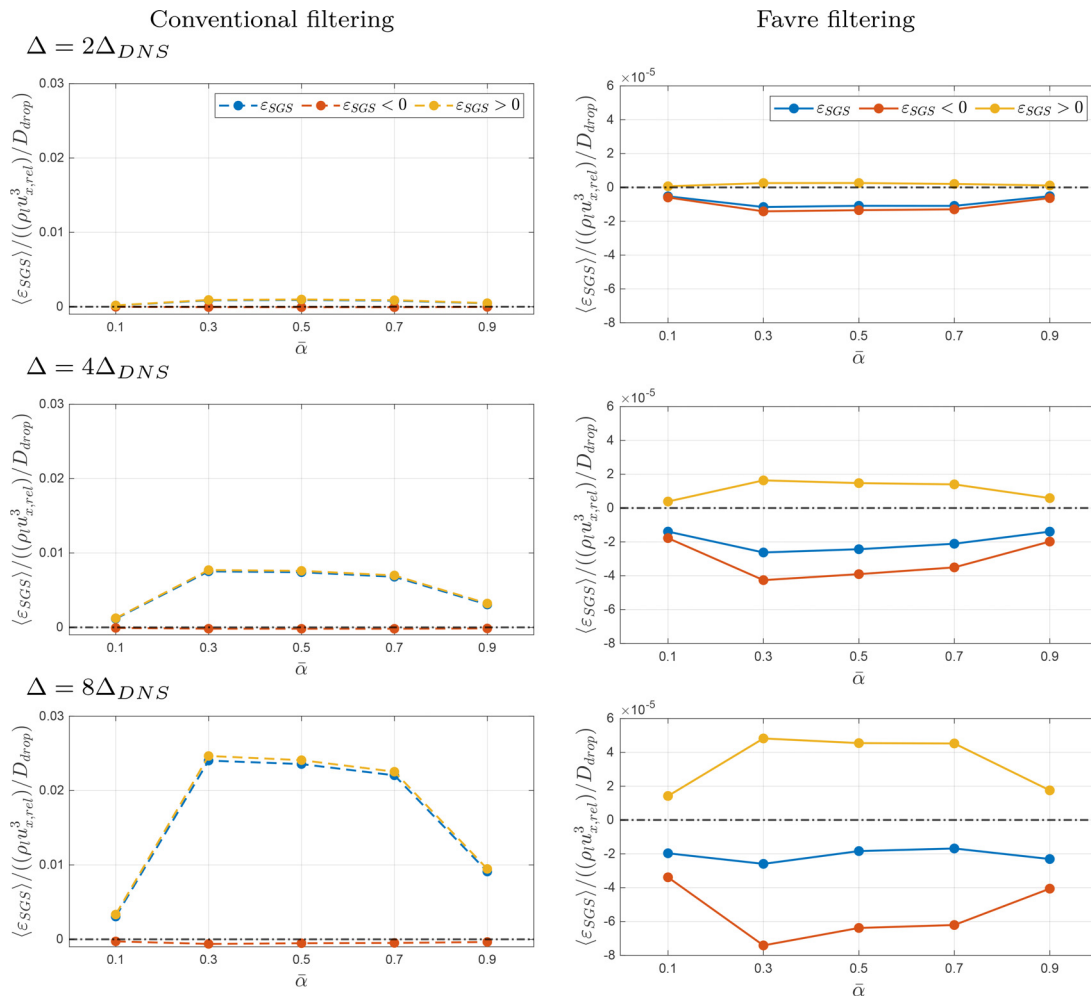


FIG. 2. Shear-thinning droplet: Total (blue), forward (red) and backward (yellow) SGS energy transfer plotted against the flow region for several filter widths. Black dash-dotted line indicates $\langle \varepsilon_{SGS} \rangle = 0$.

subgrid scales is analogous to the molecular diffusion mechanism.³¹ For the Smagorinsky model, the turbulent viscosity

$$\nu_t^s = (C_s \Delta)^2 |\tilde{S}_{ij}|, \quad |\tilde{S}_{ij}| = \sqrt{2\tilde{S}_{ij}\tilde{S}_{ij}}, \quad C_s = 0.17, \quad (26)$$

and the corresponding model constant can be derived based on the local equilibrium hypothesis and by assuming a $K^{-5/3}$ Kolmogorov spectrum with a cutoff wavenumber in the inertial range. The model constant is independent of the cutoff wavenumber K_c . This implies, that the same assumptions should be applicable to non-Newtonian flows as long as the energy spectrum has an inertial range which includes the cutoff wavenumber.

Using forced homogeneous isotropic turbulence (HIT), we investigate the $K^{-5/3}$ scaling in the inertial range of a shear-thinning fluid, which is investigated later in Sec. VB 1, see Appendix A. The results demonstrate a longer inertial range for the shear-thinning fluid compared to the Newtonian case and consequently a shift of the energy dissipation to higher wavenumbers. This suggests that the eddy

viscosity models should be applicable to shear-thinning fluids as well, with perhaps minor adjustments to the model constants. A note of caution is that the above derivation assumes isotropic homogeneous turbulence and that the situation might change for example in the vicinity of walls.

A disadvantage of the Smagorinsky model is that C_s depends on the flow configuration. In addition, the model does not vanish for laminar flow conditions and does not have the correct wall scaling. For this reason, Germano *et al.*⁴² proposed a dynamic Smagorinsky model. However, dynamic models may not be well suited for multiphase flows with a sharp interface, as they typically require spatial averaging.

Another EV model that will be included in the current analysis is the Sigma model (σ) by Nicoud *et al.*⁴³ Unlike the Smagorinsky model, the Sigma model vanishes as soon as the resolved field is either two-dimensional or two-component. Additionally, it can accurately represent the cubic scaling of ν_t close to solid boundaries, which can be beneficial regarding a certain analogy of wall-turbulence and interface-turbulence interaction.⁴⁴ The eddy viscosity reads:

$$\nu_i^\sigma = (C_\sigma \Delta)^2 \frac{\sigma_3(\sigma_1 - \sigma_2)(\sigma_3 - \sigma_2)}{\sigma_1^2}, \quad (27)$$

$$G_{ij} = \frac{\partial \tilde{u}_k}{\partial x_j} \frac{\partial \tilde{u}_k}{\partial x_i}, \quad C_\sigma = 1.35.$$

Here, σ_i are the square roots of the eigenvalues of G_{ij} and are ordered such that $\sigma_1 \geq \sigma_2 \geq \sigma_3$.

Among the structural models is a scale similarity type model for compressible flows (V-SS) proposed by Vreman *et al.*⁴⁵ The scale similarity hypothesis relies on the idea that the resolved small scales mimic the behavior of the unknown SGS scales. For variable-density flows the model reads:

$$\tau_{\rho uu,ij}^{V-SS} = \widehat{\rho \tilde{u}_i \tilde{u}_j} - \widehat{\rho} \widehat{\tilde{u}_i} \widehat{\tilde{u}_j} / \widehat{\rho}. \quad (28)$$

Here, the secondary filter operation $\widehat{\cdot}$ is performed using the filter operation by Anderson and Domaradzki,⁴⁶ as given in the following equation:

$$\widehat{\phi}_{i,j,k} = \sum_{l=-1}^{+1} \sum_{m=-1}^{+1} \sum_{n=-1}^{+1} b_l \cdot b_m \cdot b_n \cdot \phi_{i+1,j+m,k+n}. \quad (29)$$

The three dimensional filter is the product of the convolution of three one dimensional filters with the coefficients $(b_{-1}, b_0, b_{+1}) = (C, 1 - 2C, C)$. The constant C is set to 1/12.

The last model is Clark's gradient model⁴⁷ (C), which can be obtained by a Taylor series expansion of the filtered velocity. The model approximates the SGS tensor by

$$\tau_{\rho uu,ij}^C = \bar{\rho} \frac{\Delta^2}{12} \frac{\partial \tilde{u}_i}{\partial x_k} \frac{\partial \tilde{u}_j}{\partial x_k}. \quad (30)$$

Unlike the presented EV models, which only account for forward scatter, structural models try to represent the SGS tensor instead of modeling its global effect. Therefore, they are able to account for backward scatter as well. Structural models can be derived based on mathematical principles, e.g., deconvolution of the filtering operation. In addition, it can be shown in constant density flows,³¹ that, e.g., the Bardina model⁴⁸ $\tau_{ij} = \tilde{u}_i \tilde{u}_j - \tilde{u}_i \tilde{u}_j$ is equivalent to the second order gradient model $\tau_{ij} = \Delta^2 / 12 \partial \tilde{u}_i / \partial x_k \partial \tilde{u}_j / \partial x_k$.⁴⁷ For this reason structural models can be considered to be to some extent independent of the constitutive equation for the stress tensor, which could be beneficial in non-Newtonian flows.

As all previously introduced models are algebraic, it can be expected that in *a posteriori* LES their computation will consume $\approx 5\% - 10\%$ of the total computational time for one time step for an explicit projection scheme, with Vreman's scale similarity model being slightly more expensive because of the secondary filtering.⁴⁹ The

specifics of these numbers will naturally depend on the numerical scheme used and on the application in *a posteriori* LES.

V. A PRIORI ANALYSIS OF SHEAR-THINNING JET BREAKUP

This section introduces the DNS database used for the present analysis, discusses the magnitude of the unclosed terms in the momentum equation and analyzes the aforementioned of SGS closures.

A. DNS database

The following *a priori* study is based on explicit filtering of existing DNS data of shear-thinning jet breakup by Ertl and Weigand.⁸ The multiphase DNS code "Free Surface 3D" (FS3D)⁵⁰ was used for the simulations. FS3D has been developed and continuously improved for the past 30 years. The fundamental working of the code has been validated by Rieber⁵¹ against classical VOF test cases. FS3D has been used in various multiphase problems including drop-film interactions,^{52,53} drop evaporation,⁵⁴ and both Newtonian and shear-thinning jet breakup.^{9,55} The code is based on the finite volume method and solves the incompressible Navier–Stokes equations for mass and momentum conservation in the one-fluid formulation on a marker-and-cell (MAC) staggered grid. Surface tension forces are calculated using the conservative continuous surface stress model (CSS) by Lafaurie *et al.*⁵⁶ FS3D uses the VOF method to capture the interface separating the phases. The interface is reconstructed using the piecewise linear interface calculation (PLIC) method⁵⁷ to maintain a sharp interface. Ertl and Weigand⁸ used the Carreau–Yasuda model,⁴⁰ as given in Eq. (24), to account for the change in viscosity of the non-Newtonian liquid phase. The implementation of the Carreau–Yasuda viscosity model has been validated against experimental results of non-Newtonian droplet oscillations.⁵⁸

The flow configuration is a round shear-thinning jet breakup in stagnant gas. In this study, we investigate four cases, where different liquids are injected into air ($\rho_g = 1.189 \text{ kg/m}^3$, $\mu_g = 1.82 \times 10^{-5} \text{ Pa s}$): a shear-thinning case consisting of a solution of water and Praestol 2500 (referred to as P2500 0.3% later) and its corresponding pseudo-Newtonian reference case (NP2500 0.3%), and two other shear-thinning cases with different concentrations (denoted as P2500 0.8% and P2540 0.05% below). Table II provides the respective material properties for the different fluids investigated. The model parameters a , λ and n were fitted by Ertl and Weigand⁸ to experimental data provided by Ertl *et al.*⁵⁸ The investigated cases can be described using non-dimensional parameters, such as the Reynolds number $Re = \rho_l U_0 D / \mu_{l,0}$, where U_0 is the mean velocity at the inlet and D is the nozzle diameter, the Weber number $We = \rho_l U_0^2 D / \Gamma$, the density ratio ρ_l / ρ_g and the viscosity ratio $\mu_{l,0} / \mu_g$, see Table III.

TABLE II. Shear-thinning jets: Overview of the fluid properties and model parameters.

	$\rho(\text{kg/m}^3)$	$\mu_0(\text{Pa s})$	$\mu_\infty(\text{Pa s})$	$\lambda(\text{s})$	$a(-)$	$n(-)$	$\Gamma(\text{mN/m})^a$
P2500 0.3%	999.4	0.046	0.004	0.157	1.036	0.576	73.15
NP2500 0.3%	999.4	0.046	–	–	–	–	73.15
P2500 0.8%	1000.9	0.759	0.008	1.2995	1.058	0.488	75.55
P2540 0.05%	1049.2	1.59	0.005	10.065	2.842	0.266	76.51

^aSurface tension coefficient at fluid-air interface.

TABLE III. Shear-thinning jets: Non-dimensional parameters of the investigated cases.

Case	Re	We	ρ_l/ρ_g	$\mu_{l,0}/\mu_g$
P2500 0.3%	19 500	950 000	841	252.7
NP2500 0.3%	19 500	950 000	841	252.7
P2500 0.8%	118.0	891 000	842	41 703
P2540 0.05%	590	913 000	882	87 362

The computational domain is a rectangular box with the dimensions $42D \times 10D \times 10D$. The left side of the domain is a no-slip wall with a round inflow at the center. All the other sides of the domain are set to outflow boundary conditions, where Neumann boundary conditions with zero gradient for the pressure and velocity fields are prescribed. For stability reasons, negative velocities at the domain side opposite to the inflow are clipped to zero to suppress back flow. The outlet mass flow is then corrected to ensure global continuity.⁵⁹ The computational mesh has over 700×10^6 cells and a local grid refinement has been applied in the region of the jet in lateral directions extending from $3D < y < 7D$ and $3D < z < 7D$, respectively. Within the refined region, the Kolmogorov length scale η_K is of the order of the grid size. The refined mesh region up to $x = 20D$ is used for the *a priori* analysis. At the inflow, a parabolic velocity profile is superimposed by isotropic turbulent fluctuations with an integral length scale of $L_t = D/8$ and a turbulence intensity of $u'/U_0 = 0.1\%$ following the method of Huber *et al.*⁶⁰

A visualization of the investigated cases is given in Fig. 3 exemplarily for the cases P2500 0.3% and NP2500 0.3% by extracting the $\alpha = 0.5$ isocontour. The shear-thinning jet (P2500 0.3%) displays a more disturbed surface compared to the Newtonian jet (NP2500 0.3%), especially near the nozzle, where small droplets surround the core. The breakup mechanism is more enhanced for the shear-thinning case. The Newtonian jet seems to exhibit more ligaments and larger structures.

Figure 4 shows the normalized viscosity of case P2500 0.3% as an instantaneous y - x slice through the non-Newtonian jet center. The parabolic velocity profile has lower velocity gradients in the center; therefore, the viscosity is highest in the center of the jet. Higher velocity gradients at the outer part of the jet core, and thus higher shear rates

lead to a lower viscosity due to the shear-thinning behavior of the fluid. This results in a lower resistance of the liquid phase to deformation caused by interaction with the surrounding gas phase. Interface waves can be clearly observed on the jet surface in the region $5 < x/D < 10$ resulting in higher velocity gradients and therefore higher shear rates. Finally, the viscosity decreases even in the center of the jet ($x/D > 8$). Together with the merging of the shear layers, this leads to a strong breakup. Further downstream, the jet exhibits mostly ligaments and droplets.

For the present *a priori* analysis, the data have been extracted after several flow through times, after a statistically steady-state has been achieved. The field of view for the analysis corresponds to the refined mesh region extending from $3D < y < 7D$ and $3D < z < 7D$ in the lateral directions. In axial direction, the refined mesh region up to $x/D = 20$ is used. The DNS data are explicitly filtered using a variety of filter widths $\Delta = n\Delta_{DNS}$. The filtered dataset is of the same dimensions as the DNS field. In *a priori* analysis, LES model evaluation can either be carried out on the fine DNS grid or on the coarse LES grid. Liu *et al.*⁶¹ suggest that for *a priori* analysis to be meaningful, the model stress should be solely evaluated based on the coarse grid, as only variables on the coarse grid are available in a *posteriori* LES. Using filtered data sampled on the fine DNS mesh could artificially raise the level of agreement between a model and the real stress. Therefore, differentiation of closure models in the following analysis is based on the coarse grid using a second order finite difference formula, while SGS stress based on the filtered DNS is evaluated directly on the fine mesh. For a more detailed discussion the reader is referred to Klein *et al.*⁶²

B. Results and discussion

In this section, we present the results of our study. Initially, we evaluate the order of magnitude of the convective and the diffusive SGS terms. Subsequently, we assess several functional and structural LES models for closing the convective SGS term.

1. Order of magnitude of SGS terms

The order of magnitude analysis provides an initial understanding of the significance of the various SGS terms. For sufficiently high Re and consistent with earlier analysis of Newtonian jets^{5,16} where the diffusive SGS term is only nonzero at the liquid-gas interface, it could

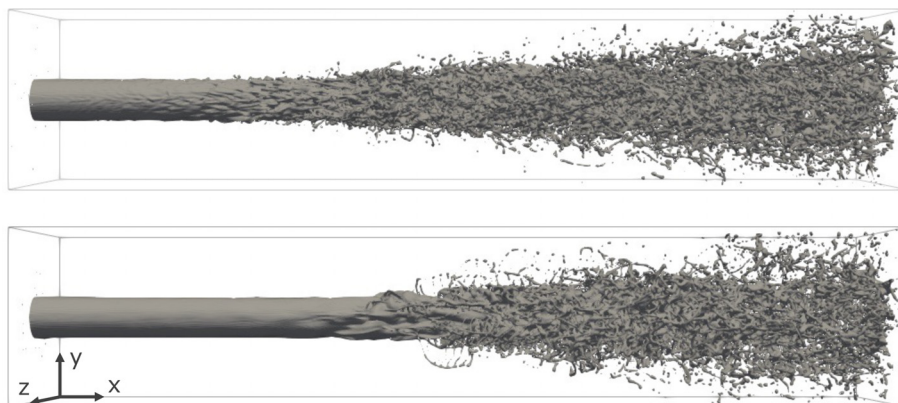


FIG. 3. Shear-thinning jets: Isocontour of investigated cases at $\alpha = 0.5$. Only the region considered for the analysis is displayed. Top: Shear-thinning case P2500 0.3%. Bottom: Newtonian reference case NP2500 0.3%.

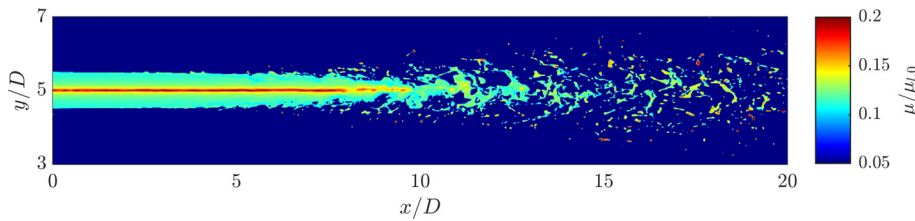


FIG. 4. Shear-thinning jets: Instantaneous two dimensional view of the normalized viscosity through the shear-thinning jet center of case P2500 0.3%.

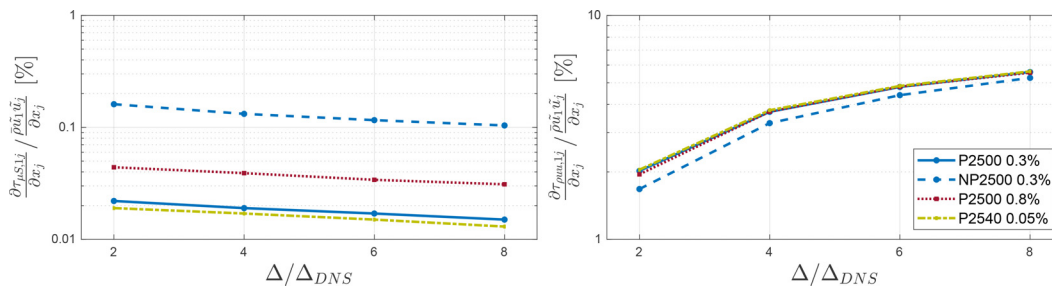


FIG. 5. Shear-thinning jets: Order of magnitude of diffusive (left) and convective (right) SGS term of the investigated cases. All terms are evaluated at the interface and in axial direction and normalized by the resolved convective term at the interface.

be expected that this SGS term plays a minor role. However, for the current setup μ can vary sharply in the vicinity of the interface, especially as we are dealing with a high viscosity ratio. Finally, due to the shear-thinning behavior of the liquid phase, this term does not vanish in the bulk liquid region.

Figure 5 shows the order of magnitude of the diffusive and convective SGS terms of the investigated cases plotted against the filter widths $\Delta/\Delta_{DNS} = 2, 4, 6$ and 8 . The terms are evaluated only at the interface and are normalized by the resolved convective term at the interface obtained from the DNS. For the sake of brevity, only the axial velocity component is considered, but the results are qualitatively similar for all other components.

Notably, the magnitude of the diffusive term shows a slight decrease with increasing filter width, while the opposite trend is observed for the convective SGS term. In case P2500 0.3%, the diffusive SGS term $\tau_{\mu S}$ is about a factor of 10 lower compared to the Newtonian reference case. This is due to the decrease in the viscosity of the liquid phase at the interface, resulting in a lower viscosity jump, which is responsible for the non-vanishing nature of this term. At the smallest filter width examined, the convective term in case P2500 0.3% surpasses the diffusive term by two orders of magnitude, underlining the small significance of the diffusive term. This trend becomes more pronounced for more realistic larger filter widths. Further, in cases P2500 0.8% and P2540 0.05%, the diffusive SGS term exhibits similarly low magnitudes. Other studies in the context of Newtonian jet breakup and phase separation have similarly demonstrated the negligible impact of the diffusive term.^{5,15}

In contrast, the convective SGS term $\tau_{\rho uu}$ exhibits a slight increase in case P2500 0.3% compared to its Newtonian reference case, highlighting the increased importance of closure models. This can be explained by the lower viscosity of the shear-thinning jet which results in an increased Reynolds number and consequently smaller SGS structures. Cases P2500 0.8% and P2540 0.05% show comparable results as case P2500 0.3%. Notably, the magnitude of $\tau_{\rho uu}$ increases with

increasing filter width, consistent with the analysis of single-phase flows by Pope,⁶³ indicating that the SGS stress scales with the filter width as $\tau \sim \Delta^{2/3}$.

Finally, the order of magnitude analysis of the diffusive term is complemented by evaluating the term in the liquid bulk region for the shear-thinning cases, see Table IV. The results have again been normalized by the resolved convective term in the liquid bulk phase. For brevity, only results in the axial direction are shown for two filter widths. It is worth mentioning that the other components follow a similar trend. Unlike in Newtonian multiphase flows, where the diffusive SGS term would vanish in the bulk phase, the term does not vanish for the shear-thinning jets. However, it can be observed that even at large filter widths this term plays a minor role in all cases. Similar observations have been made for non-Newtonian single-phase flows in the literature.²³ Compared to the magnitude of this term at the interface, see Fig. 5, the diffusive SGS term is about 1–2 orders of magnitude smaller in the liquid bulk regions.

2. Closure of convective SGS term

Closure models for the convective SGS term have been introduced in Sec. IV. To assess these closure models, we calculate the Pearson correlation coefficient and the Euclidean L_2 -norm. The

TABLE IV. Shear-thinning jets: Order of magnitude of the diffusive term in the liquid bulk region in the axial direction normalized by the resolved convective term in the liquid bulk phase.

	$\Delta = 2\Delta_{DNS}$	$\Delta = 8\Delta_{DNS}$
P2500 0.3%	0.0006%	0.0018%
P2500 0.8%	0.0018%	0.0076%
P2540 0.05%	0.0003%	0.0009%

analysis is limited to the case P2500 0.3% and its Newtonian reference case NP2500 0.3%. The results for the other shear-thinning jets are very similar and do not provide additional insight. Both correlation analysis and L_2 -norm calculations are performed across various filter widths and flow regions.

The correlation analysis is conducted on tensor level and on vector level after taking the divergence of the convective SGS term. The Pearson correlation coefficient is a measure for the linear correlation between τ and τ^m and takes values between -1 and $+1$. A value of $+1$ corresponds to a total positive linear correlation, 0 is no linear correlation and -1 is a total negative linear correlation. To validate the quality of an SGS closure model, it is desirable for the correlations to approach $+1$. The Pearson correlation coefficient PCC is defined as

$$PCC = \frac{Cov(\tau, \tau^m)}{\sqrt{Var(\tau)}\sqrt{Var(\tau^m)}}, \quad (31)$$

where Cov denotes the covariance, and Var is the variance. Values obtained from explicitly filtered DNS and values predicted by the corresponding model are denoted by τ and τ^m , respectively.

Figure 6 shows the correlation analysis for the shear-thinning case plotted against varying filter widths for the entire investigated flow field. Structural models, such as Vreman’s scale similarity type model (V-SS) and Clark’s gradient model (C), and functional closure models, i.e., the standard Smagorinsky model (S) and Nicoud’s sigma model (σ), are compared. On tensor level, exemplarily shown here for two diagonal components $\tau_{\rho uu,11}$ and $\tau_{\rho uu,22}$ (other components show very similar behavior) both structural models exhibit strong correlations across all filter widths. This can be explained by the specific structure of these models, as they can be derived based on mathematical principles (i.e., Taylor series expansion of the filter), which are independent of the constitutive equation for the shear stress. Vreman’s scale similarity model overall gives the best performance. On the contrary, functional models display weaker correlations ($\rho < 0.4$). This behavior is observed as well in other studies conducted for both multiphase flows^{3,5} and single-phase flows.⁴⁷ As the filtered momentum equation, see Eq. (18), incorporates the divergence of $\tau_{\rho uu,ij}$ rather than the tensor itself, the correlation analysis is shown here exemplarily in the axial direction on vector level, as this is the dominating component. The correlation coefficients deteriorate for all models after taking the divergence of $\tau_{\rho uu,ij}$, particularly at large filter widths, due to differentiation errors.⁶² At larger filter widths, Clark’s model slightly outperforms the other models.

Next, the correlation analysis is extended to compare the shear-thinning and its Newtonian case reference conditionally for different flow regions for $\Delta = 4\Delta_{DNS}$, as depicted in Fig. 7. The flow domain is divided in five flow regions, where the gas bulk phase and the liquid bulk phase are denoted by “g” and “l,” respectively. The interface is marked by “i.” The regions approaching the interface from the gas side are denoted by “g/i,” while the region approaching the liquid phase from the interface is denoted by “i/l.” The two latter regions surround the interface with a thickness of the same order as the filter size. This enables a more detailed evaluation of the closure models in the different flow regions, particularly in the liquid phase where the viscosity is changing with the shear rate. The correlation analysis is shown exemplarily for the diagonal component τ_{11} . In both the Newtonian and shear-thinning scenarios, Vreman’s scale similarity model and Clark’s model follow a similar trend, particularly when approaching the liquid

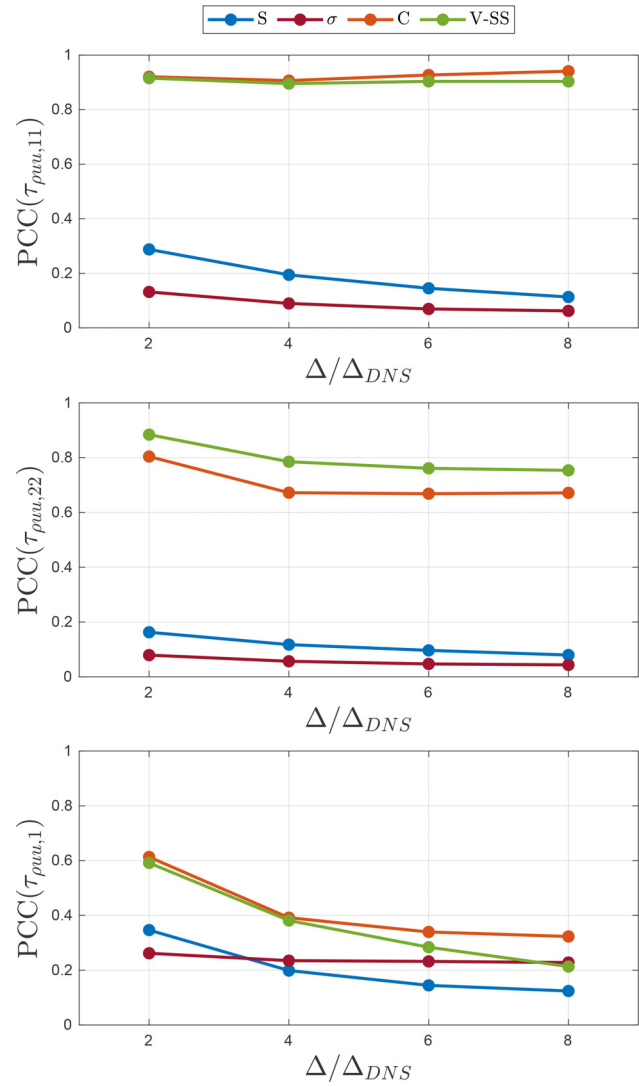


FIG. 6. Shear-thinning jets: Correlation analysis of closure models for the convective SGS term conducted on tensor level for $\tau_{\rho uu,11}$ and $\tau_{\rho uu,22}$ (top and middle) and on vector level for $\tau_{\rho uu,1}$ (bottom) for the shear-thinning case (P2500 0.3%) plotted against the filter width.

bulk flow. Notably, the correlation of Vreman’s structural model with the actual SGS stress deteriorates in the “g/i” region, consistent with the study by Klein *et al.*⁵ As observed earlier, the EV models show poor correlations across all flow regions for both Newtonian and shear-thinning case. In particular, it is noted that a counter-gradient transport is observed in the gas phase for this particular component of the SGS stress. The higher correlations of the models for the liquid side can be explained by the fact that the liquid Reynolds number is lower than the gas Reynolds number, resulting in a reduced amount of subgrid activity.

The correlation coefficient is invariant with respect to multiplication of the model with a constant. Hence, it cannot be used to evaluate the magnitude of the unclosed terms. Instead, this can be evaluated using the L_2 -norm, defined as follows:

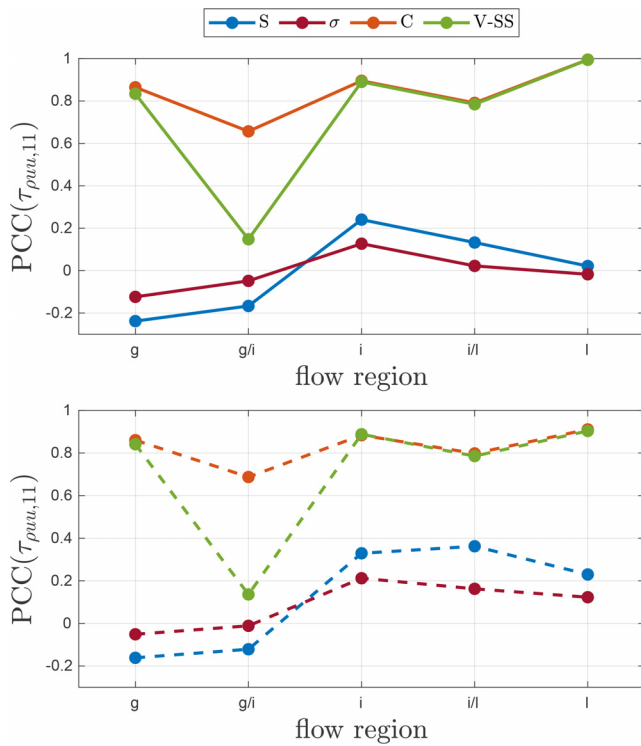


FIG. 7. Shear-thinning jets: Correlation analysis of closure models for the convective SGS term conducted on tensor level for $\tau_{\rho uu,11}$ plotted against the flow region for $\Delta = 4\Delta_{DNS}$. Top: Shear-thinning case (P2500 0.3%). Bottom: Newtonian case (NP2500 0.3%).

$$\|\tau\|_2 = \sqrt{\langle \tau^2 \rangle}. \quad (32)$$

Figure 8 depicts the L_2 -norm of the convective SGS term on tensor level at a filter width of $\Delta = 4\Delta_{DNS}$ across different flow regions. The magnitude of the filtered DNS, as well as the closure models, are shown for both Newtonian and shear-thinning cases. The results are given for one diagonal component of the SGS stress, namely τ_{11} . Structural models show a similar trend in both Newtonian and shear-thinning cases, while functional models tend to under-predict the actual stress across the different flow regions. In the shear-thinning case, the discrepancy between the magnitude of the filtered DNS and the predicted stress from EV models increases, particularly in the liquid bulk phase, as these models only model the deviatoric part of the stress tensor.

The results of the *a priori* analysis show a good performance of the structural models on tensor and vector level. However, structural models often become unstable in *a posteriori* studies, because they are not dissipative enough.⁵ In this context it is worth mentioning, that Klein *et al.*⁶⁴ suggested a parameter-free modeling strategy to combine structural and functional models by avoiding undesirable backward scatter. Vreman *et al.*⁶⁵ applied a dynamic procedure to the original Clark model for stabilization. Recently, Hasslberger⁶⁶ suggested a sensor-based mixed model using the Smagorinsky model and Clark’s gradient model.

VI. CONCLUSION

In this study, we compared two filtering approaches, namely, the conventional filtering method and the Favre filtering method, using an

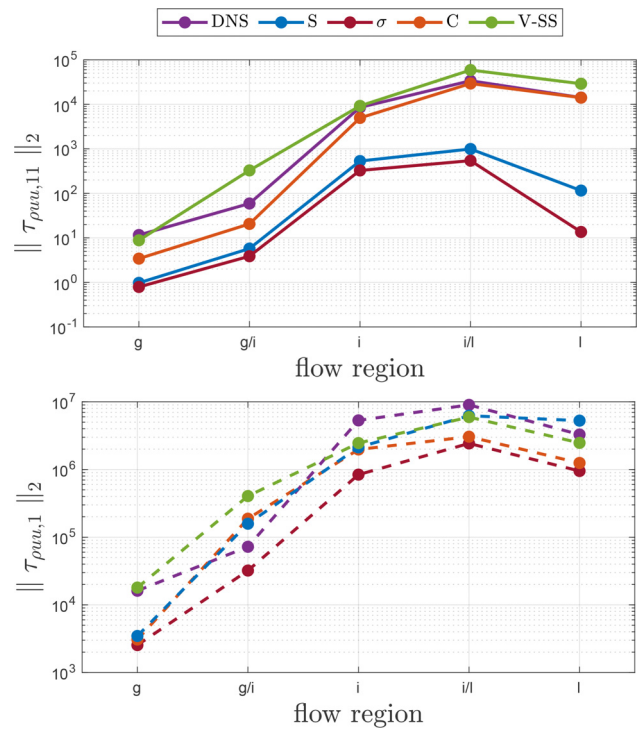


FIG. 8. Shear-thinning jets: L_2 -norm of the convective SGS term at tensor level plotted across different flow regions at moderate filter width $\Delta = 4\Delta_{DNS}$. Top: shear-thinning case (P2500 0.3%). Bottom: Newtonian case (NP2500 0.3%).

a priori analysis of a shear-thinning droplet to determine which approach is more suitable for LES modeling of two-phase flow. By analyzing the SGS energy transfer conditional at the interface, we found that the conventional filtering approach is less suitable, as it results in an excessive amount of backward scatter, which is not in agreement with the common LES modeling assumptions.

By using the Favre filtered formulation of the LES governing equations in the one-fluid formulation, several unclosed SGS terms have been investigated for shear-thinning and Newtonian liquid jets. In Newtonian two-phase flows, the diffusive SGS term exists only at the interface due to the discontinuity of the viscosity. However, when dealing with shear-thinning flows, the diffusive SGS term does not vanish in the non-Newtonian bulk phase. An order of magnitude analysis shows, that the diffusive term at the interface and in the shear-thinning bulk phase can be neglected for the investigated cases. However, it was shown that the magnitude of the unclosed convective SGS term increases in the shear-thinning cases, and this trend increases with increasing Reynolds number, underlining the importance of a high-fidelity closure model. Therefore, several SGS models have been evaluated for the convective SGS term in terms of a correlation analysis and their order of magnitude. The results have shown accurate performance of the structural models in both shear-thinning and Newtonian cases. Conversely, functional models showed marginally inferior performance for the shear-thinning jet compared to the Newtonian reference case, as they are directly dependent on the shear rate.

In fact, simulations of shear-thinning fluids in linearly forced isotropic turbulence have demonstrated a longer inertial range compared

to the Newtonian case, and consequently a shift of the energy dissipation to higher wavenumbers. This suggests that the eddy viscosity models (away from walls) should in principal be applicable to shear-thinning fluids as well, with perhaps minor adjustments to the model constants.

The findings indicate that functional models, without any modifications, might be less suitable for non-Newtonian two-phase LES. As the dynamic procedure will be difficult to apply to two-phase flows due to the moving sharp interface (because of the required regularization), a Lagrangian dynamic procedure applied conditionally to the respective phases could be an alternative option in future *a posteriori* LES. Since the present *a priori* analysis indicates similar behavior of SGS closures for Newtonian and shear-thinning cases, existing mixed models might offer a promising compromise in *a posteriori* LES of shear-thinning two-phase flow, as structural models tend not to be dissipative enough. Addressing these questions forms the basis of our future work.

ACKNOWLEDGMENTS

The authors greatly acknowledge financial support of this project from the German Research Foundation (Deutsche Forschungsgemeinschaft—DFG Project No. 503977784). Computational resources (HPC-cluster HSUper) have been provided by the project hpc.bw, funded by dtec.bw—Digitalization and Technology Research Center of the Bundeswehr. dtec.bw is funded by the European Union—NextGenerationEU.

AUTHOR DECLARATIONS

Conflict of Interest

The authors have no conflicts to disclose.

Author Contributions

M. Abdelsayed: Conceptualization (equal); Data curation (equal); Formal analysis (lead); Methodology (equal); Visualization (lead); Writing – original draft (lead). **J. Hasslberger:** Conceptualization (equal); Methodology (equal); Writing – review & editing (equal). **M. Ertl:** Data curation (equal); Writing – review & editing (equal). **B. Weigand:** Funding acquisition (equal); Writing – review & editing (equal). **M. Klein:** Conceptualization (equal); Funding acquisition (equal); Methodology (equal); Supervision (lead); Writing – review & editing (equal).

DATA AVAILABILITY

The data that support the findings of this study are available from the corresponding author upon reasonable request.

NOMENCLATURE

Greek symbols

α	Local volume fraction
Γ	Surface tension coefficient
$\dot{\gamma}$	Shear rate
Δ	Filter width

δ_S	Interface indicator function
ε	Dissipation rate
ε_{SGS}	Subgrid scale energy transfer
η_K	Kolmogorov length scale
κ	Local interface curvature
λ	Characteristic time
μ	Dynamic viscosity
μ_0	First Newtonian plateau
μ_∞	Second Newtonian plateau
ν	Kinematic viscosity
ν_t	Turbulent viscosity
ρ	Density
σ_i	Square roots of the eigenvalues of G_{ij}
τ	Subgrid scale stress
ϕ	Field variable

Roman Symbols

A	Forcing parameter
a	Transition between Newtonian plateau and power-law
C_S	Smagorinsky model constant
C_σ	Sigma model constant
D	Nozzle diameter
D_{drop}	Droplet diameter
E	Turbulent kinetic energy spectrum
G	Gaussian filter kernel
g_i	Gravitational acceleration
K	Wavenumber
K_c	Cutoff wavenumber
K_0	Lowest non-zero wavenumber
k	Turbulent kinetic energy
k_0	Desired turbulent kinetic energy
L	Domain length
L_t	Integral length scale
n	Power-law index
n_i	Unit vector normal to interface
p	Pressure
S_{ij}	Strain rate tensor
t	Time
U_0	Mean velocity at the inlet
u'	Velocity fluctuations
u_i	Velocity vector
x_i	Position vector

Subscripts

l	Liquid phase
g	Gas phase

APPENDIX: FORCED HOMOGENEOUS ISOTROPIC TURBULENCE

The Lundgren linear forcing method⁶⁷ is used to investigate the energy spectrum in the inertial region of forced HIT of shear-thinning single-phase flows. The open-source code PARIS³⁷ was used for this study. Forcing in physical space is achieved by applying an external force to the Navier–Stokes equations. The governing equations are given as

$$\frac{\partial u_i}{\partial x_i} = 0, \tag{A1}$$

$$\rho \left(\frac{\partial u_i}{\partial t} + \frac{\partial u_i u_j}{\partial x_j} \right) = - \frac{\partial p}{\partial x_i} + \frac{\partial}{\partial x_j} \left[\mu \left(\frac{\partial u_i}{\partial x_j} + \frac{\partial u_j}{\partial x_i} \right) \right] + A u_i, \tag{A2}$$

where A is the forcing parameter, which controls the amount of energy added to the velocity field. It is derived from the turbulent kinetic energy equation

$$\frac{dk}{dt} = -\varepsilon + 2Ak, \tag{A3}$$

where $dk/dt = 0$ for a statistically stationary state. Here, k is the turbulent kinetic energy (TKE) and ε is the dissipation rate. Carroll and Blanquart⁶⁸ proposed a modification to Lundgren's forcing term, allowing a faster convergence to a desired TKE k_0 . The modified forcing term A then reads

$$A = \frac{\varepsilon k_0}{2k k}. \tag{A4}$$

Two configurations are considered in this study, a shear-thinning case (P2500 0.8%) and its Newtonian reference case (NP2500 0.8%). The Carreau-Yasuda model⁴⁰ is used to model the viscous behavior of the fluid. The fluid parameters, such as density and viscosity model parameters are given in Table IV in Sec. V B 1.

The computational domain is a triply periodic box with a length of $L = 2\pi$ and 1024^3 cells. The grid resolution is of the order of the Kolmogorov length scale η_K . In the shear-thinning case, $\eta_K = ((\nu)^3 / \langle \varepsilon \rangle)^{1/4} = 1.11 \cdot \Delta$, whereas in the Newtonian case, $\eta_K = 2.17 \cdot \Delta$. The desired TKE is set to $k_0 = 0.1 \text{ m}^2/\text{s}^2$ for both investigated cases.

Figure 9 depicts the one dimensional energy spectra E_{11} for both investigated cases normalized by the lowest non-zero wavenumber $K_0 = 2\pi/L$. A clear $E \sim K^{-5/3}$ scaling can be observed for both cases in the inertial range, while the non-Newtonian case exhibits a larger inertial range, as the Reynolds number based on the Taylor microscale Re_λ is higher for the latter.

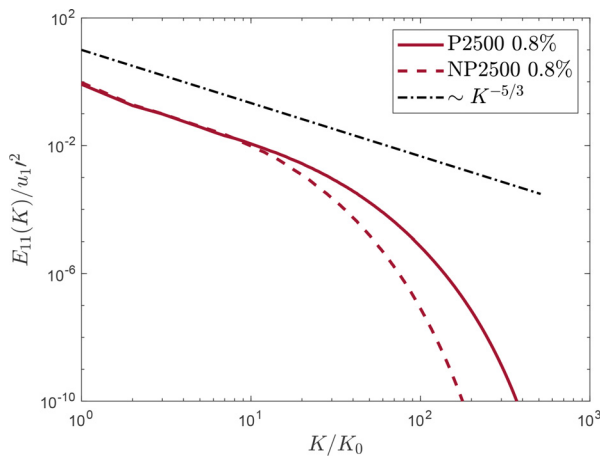


FIG. 9. Forced homogeneous isotropic turbulence: One dimensional turbulent kinetic energy spectra E_{11} of the investigated cases.

REFERENCES

- ¹A. Lefebvre, *Atomization and Sprays* (CRC Press Inc., 1989).
- ²M. Herrmann, "On simulating primary atomization using the refined level set grid method," *Atomization Sprays* **21**, 283–301 (2011).
- ³S. Ketterl and M. Klein, "A-priori assessment of subgrid scale models for large-eddy simulation for multiphase primary breakup," *Comput. Fluids* **165**, 64–77 (2018).
- ⁴J. Hasslberger, S. Ketterl, M. Klein, and N. Chakraborty, "Flow topologies in primary atomization of liquid jets: A direct numerical simulation analysis," *J. Fluid Mech.* **859**, 819–838 (2019).
- ⁵M. Klein, S. Ketterl, and J. Hasslberger, "Large eddy simulation of multiphase flows using the volume of fluid method: Part 1—Governing equations and a priori analysis," *Exp. Comput. Multiphase Flow* **1**, 130–144 (2019).
- ⁶C. Pairetti, S. M. Damián, N. M. Nigro, S. Popinet, and S. Zaleski, "Mesh resolution effects on primary atomization simulations," *Atomization Sprays* **30**, 913–935 (2020).
- ⁷E. Trautner, J. Hasslberger, S. Ketterl, and M. Klein, "Primary atomization of liquid jets: Identification and investigation of droplets at the instant of their formation using direct numerical simulation," *Int. J. Multiphase Flow* **160**, 104360 (2023).
- ⁸M. Ertl and B. Weigand, "Analysis methods for direct numerical simulations of primary breakup of shear-thinning liquid jets," *Atomization Sprays* **27**, 303–317 (2017).
- ⁹C. Zhu, M. Ertl, and B. Weigand, "Numerical investigation on the primary breakup of an inelastic non-Newtonian liquid jet with inflow turbulence," *Phys. Fluids* **25**, 083102 (2013).
- ¹⁰G. Soligo and M. E. Rosti, "Non-Newtonian turbulent jets at low-Reynolds number," *Int. J. Multiphase Flow* **167**, 104546 (2023).
- ¹¹M. C. Guimarães, N. Pimentel, F. T. Pinho, and C. B. da Silva, "Direct numerical simulations of turbulent viscoelastic jets," *J. Fluid Mech.* **899**, A11 (2020).
- ¹²E. Labourasse, D. Lacanette, A. Toutant, P. Lubin, S. Vincent, O. Lebaigue, J. P. Caltagirone, and P. Sagaut, "Towards large eddy simulation of isothermal two-phase flows: Governing equations and a priori tests," *Int. J. Multiphase Flow* **33**, 1–39 (2007).
- ¹³P. Liovic and D. Lakehal, "Subgrid-scale modelling of surface tension within interface tracking-based Large Eddy and Interface Simulation of 3D interfacial flows," *Comput. Fluids* **63**, 27–46 (2012).
- ¹⁴A. Toutant, E. Labourasse, O. Lebaigue, and O. Simonin, "DNS of the interaction between a deformable buoyant bubble and a spatially decaying turbulence: A priori tests for LES two-phase flow modelling," *Comput. Fluids* **37**, 877–886 (2008).
- ¹⁵S. Vincent, M. Tavares, S. Fleau, S. Mimouni, M. Ould-Rouiss, and J.-L. Estivalezes, "A priori filtering and LES modeling of turbulent two-phase flows application to phase separation," *Comput. Fluids* **176**, 245–259 (2018).
- ¹⁶J. Chesnel, T. Menard, J. Reveillon, and F.-X. Demoulin, "Subgrid analysis of liquid jet atomization," *Atomization Sprays* **21**, 41–67 (2011).
- ¹⁷W. Aniszewski, A. Bogusławski, M. Marek, and A. Tyliczszak, "A new approach to sub-grid surface tension for LES of two-phase flows," *J. Comput. Phys.* **231**, 7368–7397 (2012).
- ¹⁸S. Stolz and N. A. Adams, "An approximate deconvolution procedure for large-eddy simulation," *Phys. Fluids* **11**, 1699–1701 (1999).
- ¹⁹M. Saeedipour, S. Vincent, and S. Pirker, "Large eddy simulation of turbulent interfacial flows using approximate deconvolution model," *Int. J. Multiphase Flow* **112**, 286–299 (2019).
- ²⁰M. Saeedipour and S. Schneiderbauer, "A new approach to include surface tension in the subgrid eddy viscosity for the two-phase LES," *Int. J. Multiphase Flow* **121**, 103128 (2019).
- ²¹J. Hasslberger, S. Ketterl, and M. Klein, "A-priori assessment of interfacial sub-grid scale closures in the two-phase flow LES context," *Flow, Turbul. Combust.* **105**, 359–375 (2020).
- ²²S. Ketterl, M. Reißmann, and M. Klein, "Large eddy simulation of multiphase flows using the volume of fluid method: Part 2—A-posteriori analysis of liquid jet atomization," *Exp. Comput. Multiphase Flow* **1**, 201–211 (2019).
- ²³T. Ohta and M. Miyashita, "DNS and LES with an extended Smagorinsky model for wall turbulence in non-Newtonian viscous fluids," *J. Non-Newtonian Fluid Mech.* **206**, 29–39 (2014).

- ²⁴P. S. Gnanbode, P. Orlandi, M. Ould-Rouiss, and X. Nicolas, "Large-Eddy simulation of turbulent pipe flow of power-law fluids," *Int. J. Heat Fluid Flow* **54**, 196–210 (2015).
- ²⁵E. Amani, A. Ahmadpour, and M. J. Aghajari, "Dynamic subgrid-scale LES model for turbulent non-Newtonian flows: A priori and a posteriori analyses of Burgers turbulence," *J. Non-Newtonian Fluid Mech.* **295**, 104615 (2021).
- ²⁶L. Thais, A. E. Tejada-Martínez, T. B. Gatski, and G. Mompean, "Temporal large eddy simulations of turbulent viscoelastic drag reduction flows," *Phys. Fluids* **22**, 013103 (2010).
- ²⁷M. Masoudian, C. B. da Silva, and F. T. Pinho, "Grid and subgrid-scale interactions in viscoelastic turbulent flow and implications for modelling," *J. Turbul.* **17**, 543–571 (2016).
- ²⁸P. O. Ferreira, F. T. Pinho, and C. B. da Silva, "Large-eddy simulations of forced isotropic turbulence with viscoelastic fluids described by the FENE-P model," *Phys. Fluids* **28**, 125104 (2016).
- ²⁹G. Tryggvason, R. Scardovelli, and S. Zaleski, *Direct Numerical Simulations of Gas-Liquid Multi-Phase Flows* (Cambridge University Press, 2011).
- ³⁰C. W. Hirt and B. D. Nichols, "Volume of Fluid (VOF) Method for the dynamics of free boundaries," *J. Comput. Phys.* **39**, 201–225 (1981).
- ³¹P. Sagaut, *Large Eddy Simulation for Incompressible Flows* (Springer Berlin Heidelberg, 2002).
- ³²A. Favre, "Statistical equations of turbulent gases," in *Problems of Hydrodynamic and Continuum Mechanics* (SIAM, Philadelphia, PA, 1969).
- ³³P. Liovic and D. Lakehal, "Multi-physics treatment in the vicinity of arbitrarily deformable gas-liquid interfaces," *J. Comput. Phys.* **222**, 504–535 (2007).
- ³⁴E. Garnier, N. Adams, and P. Sagaut, *Large Eddy Simulation for Compressible Flows* (Springer Dordrecht, 2009).
- ³⁵T. Poinso and D. Veynante, *Theoretical and Numerical Combustion* (R.T. Edwards, 2005).
- ³⁶L. Richardson, *Weather Prediction by Numerical Process* (Cambridge University Press, 1922).
- ³⁷W. Aniszewski, T. Arrufat, M. Cialesi-Esposito, S. Dabiri, D. Fuster, Y. Ling, J. Lu, L. Malan, S. Pal, R. Scardovelli, G. Tryggvason, P. Yecko, and S. Zaleski, "PARALLEL, Robust, Interface Simulator (PARIS)," *Comput. Phys. Commun.* **263**, 107849 (2021).
- ³⁸R. Scardovelli and S. Zaleski, "Interface reconstruction with least-square fit and split Eulerian-Lagrangian advection," *Int. J. Numer. Methods Fluids* **41**, 251–274 (2003).
- ³⁹M. Koebe, D. Bothe, and H.-J. Warnecke, "Direct numerical simulation of air bubbles in water/glycerol mixtures: Shapes and velocity fields," in *Proceedings of the ASME/JSME 4th Joint Fluids Engineering Conference* (ASME, 2003), pp. 415–421.
- ⁴⁰R. Tanner, *Engineering Rheology* (Oxford University Press, 2000).
- ⁴¹J. Smagorinsky, "General circulation experiments with the primitive equations," *Mon. Weather Rev.* **91**, 99–164 (1963).
- ⁴²M. Germano, U. Piomelli, P. Moin, and W. H. Cabot, "A dynamic subgrid-scale eddy viscosity model," *Phys. Fluids* **3**, 1760–1765 (1991).
- ⁴³F. Nicoud, H. Toda, O. Cabrit, S. Bose, and J. Lee, "Using singular values to build a subgrid-scale model for large eddy simulations," *Phys. Fluids* **23**, 085106 (2011).
- ⁴⁴M. Fulgosi, D. Lakehal, S. Banerjee, and V. De Angelis, "Direct numerical simulation of turbulence in a sheared air-water flow with a deformable interface," *J. Fluid Mech.* **482**, 319–345 (2003).
- ⁴⁵B. Vreman, B. Geurts, and H. Kuerten, "A priori tests of large eddy simulation of the compressible plane mixing layer," *J. Eng. Math.* **29**, 299–327 (1995).
- ⁴⁶B. W. Anderson and J. A. Domaradzki, "A subgrid-scale model for large-eddy simulation based on the physics of interscale energy transfer in turbulence," *Phys. Fluids* **24**, 065104 (2012).
- ⁴⁷R. A. Clark, J. H. Ferziger, and W. C. Reynolds, "Evaluation of subgrid-scale models using an accurately simulated turbulent flow," *J. Fluid Mech.* **91**, 1–16 (1979).
- ⁴⁸J. Bardina, "Improved turbulence models based on large eddy simulation of homogeneous, incompressible turbulent flows," Ph.D. Dissertation (Stanford University, 1983).
- ⁴⁹L. Engelmann, J. Hasslberger, E. Inanc, M. Klein, and A. Kempf, "A-posteriori assessment of Large-Eddy Simulation subgrid-closures for momentum and scalar fluxes in a turbulent premixed burner experiment," *Comput. Fluids* **240**, 105441 (2022).
- ⁵⁰K. Eisenschmidt, M. Ertl, H. Gomma, C. Kieffer-Roth, C. Meister, P. Rauschenberger, M. Reitzle, K. Schlottke, and B. Weigand, "Direct numerical simulations for multi-phase flows: An overview of the multi-phase code FS3D," *Appl. Math. Comput.* **272**, 508–517 (2016).
- ⁵¹M. Rieber, *Numerische Modellierung der Dynamik Freier Grenzflächen in Zweiphasenströmungen* (University of Stuttgart, 2004).
- ⁵²J. Kaufmann, A. Geppert, M. Ertl, R. Bernard, V. Vaikuntanathan, G. Lamanna, and B. Weigand, "Direct numerical simulations of one- and two-component droplet wall-film interactions within the crown-type splashing regime," in 14th Triennial International Conference on Liquid Atomization and Spray Systems (ICLASS), Chicago, IL, 2018.
- ⁵³S. Fest-Santini, J. Steigerwald, M. Santini, G. E. Cossali, and B. Weigand, "Multiple drops impact onto a liquid film: Direct numerical simulation and experimental validation," *Comput. Fluids* **214**, 104761 (2021).
- ⁵⁴J. Reutzsch, C. Kieffer-Roth, and B. Weigand, "A consistent method for direct numerical simulation of droplet evaporation," *J. Comput. Phys.* **413**, 109455 (2020).
- ⁵⁵H. Gomma, S. Kumar, C. Huber, B. Weigand, and B. Peters, "Numerical comparison of 3D jet breakup using a compression scheme and an interface reconstruction based VOF-code," in Proceedings of the 24th European Conference on Liquid Atomization and Spray Systems (ILASS Europe), Estoril, Portugal, 2011.
- ⁵⁶B. Lafaurie, C. Nardone, R. Scardovelli, S. Zaleski, and G. Zanetti, "Modelling merging and fragmentation in multiphase flows with SURFER," *J. Comput. Phys.* **113**, 134–147 (1994).
- ⁵⁷W. J. Rider and D. B. Kothe, "Reconstructing volume tracking," *J. Comput. Phys.* **141**, 112–935 (1998).
- ⁵⁸M. Ertl, N. Roth, G. Brenn, H. Gomma, and B. Weigand, "Simulations and experiments on shape oscillations of Newtonian and non-Newtonian liquid droplets," in ILASS, 2013.
- ⁵⁹M. Ertl, "Direct numerical investigations of Non-Newtonian drop oscillations and jet breakup," Ph.D. thesis (University of Stuttgart, 2019).
- ⁶⁰C. Huber, H. Gomma, and B. Weigand, "Application of a novel turbulence generator to multiphase flow computations," in *High Performance Computing in Science and Engineering '10*, edited by W. E. Nagel, D. B. Kröner, and M. M. Resch (Springer Berlin Heidelberg, Berlin, Heidelberg, 2011), pp. 273–286.
- ⁶¹S. Liu, C. Meneveau, and J. Katz, "On the properties of similarity subgrid-scale models as deduced from measurements in a turbulent jet," *J. Fluid Mech.* **275**, 83–119 (1994).
- ⁶²M. Klein, N. Chakraborty, and Y. Gao, "Scale similarity based models and their application to subgrid scale scalar flux modelling in the context of turbulent premixed flames," *Int. J. Heat Fluid Flow* **57**, 91–108 (2016).
- ⁶³S. Pope, *Turbulent Flows* (Cambridge University Press, 2000).
- ⁶⁴M. Klein, S. Ketterl, L. Engelmann, A. Kempf, and H. Kobayashi, "Regularized, parameter free scale similarity type models for Large Eddy Simulation," *Int. J. Heat Fluid Flow* **81**, 108496 (2020).
- ⁶⁵B. Vreman, B. Geurts, and H. Kuerten, "Large-eddy simulation of the temporal mixing layer using the Clark model," *Theor. Comput. Fluid Dyn.* **8**, 309–324 (1996).
- ⁶⁶J. Hasslberger, "Dynamic mixed modeling in large eddy simulation using the concept of a subgrid activity sensor," *Fluids* **8**, 219 (2023).
- ⁶⁷T. Lundgren, "Linearly forced isotropic turbulence," in Center for Turbulence Research Annual Research Briefs, 2003, Vol. 461–473.
- ⁶⁸P. L. Carroll and G. Blanquart, "A proposed modification to Lundgren's physical space velocity forcing method for isotropic turbulence," *Phys. Fluids* **25**, 105114 (2013).